ISSN 0021-8944, Journal of Applied Mechanics and Technical Physics, 2020, Vol. 61, No. 4, pp. 676–684. © Pleiades Publishing, Ltd., 2020.
Original Russian Text © L.F. Yu, Z.G. Zuo, L. Li, S.H. Liu, S.T. Zhao.

# EXPERIMENTAL BREAKUP CHARACTERISTICS OF ROUND LIQUID JETS OF A DILUTE POLYMER SOLUTION INTO QUIESCENT AIR

**L. F. Yu[a], Z. G. Zuo[b,*], L. Li[a,*], S. H. Liu[b], and S. T. Zhao[a]**

UDC 532.5, 677.494

**Abstract:** Experiments are performed on dilute polymer solutions jetting into quiescent air with a jet velocity range of 30–87 m/s. Polymer solutions are those with several hundred ppm concentrations of long-chain polyoxyethylene (millions of molecular weight) dissolved in purified water. The breakup characteristics of the jets were recorded by high-speed photography from four observation windows along the jet direction. The breakup morphologies of dilute polymer solution jets are significantly different from that of Newtonian fluids. Small-scale interfacial disturbances are suppressed, while a twisted liquid column waving with large amplitudes is observed. When the jet velocity exceeds a critical value, liquid films and filaments are peeled off successively from the liquid column. Four different breakup patterns are distinguished. The diameters of the central liquid column and the principal liquid filament are observed to decrease with increasing jet velocity.

*Keywords:* polymer, round jet, breakup pattern, interfacial disturbance, unrelaxed stresses.

**DOI:** 10.1134/S0021894420040227

## INTRODUCTION

In recent years, the interest in non-Newtonian fluid jet breakup has grown tremendously. Liquid solutions with small amounts of high-molecular-weight polymers or biological macromolecules exhibit viscoelastic features [1]. Viscoelastic liquid jets are common in various engineering fields, e.g., laser inkjet printing [2], coating spraying [3], agricultural chemicals sprays [4], and electrospinning [5]. It is known that the breakup of a high-speed Newtonian liquid jet starts with the nonlinear growth of disturbances caused by the aerodynamic interaction arising from the relative motion between the jet and the surrounding gas. These unstable growing waves (usually with very short axial wavelengths) nonlinearly interact downstream, leading to a complex turbulent behavior, and eventually break the liquid jet into ligaments and droplets [6]. Compared to Newtonian liquid jets, the mechanisms of viscoelastic liquid jets are more complicated. The constitutive relation of the viscoelastic fluid is complex because nonlinear behaviors like shear thinning and strain hardening emerge [7]. Elastic stresses are formed in flow domains in which the shear rate or the extensional rate exceeds a critical value. To investigate the mechanisms of the breakup of viscoelastic jets, many researchers made significant theoretical and experimental contributions to the dynamical mechanisms of droplet formation and of capillary jets, as well as the droplet-size distribution of viscoelastic fluids.

[a]Research Institute of Chemical Defence, Beijing, China; fhyulf86@163.com; *rockysys_15@163.com; zhaoshoutian@yeah.net. [b]State Key Laboratory of Hydro Science and Engineering, Department of Energy and Power Engineering, Tsinghua University, Beijing, China; *zhigang200@tsinghua.edu.cn; liushuhong@tsinghua.edu.cn.
Translated from Prikladnaya Mekhanika i Tekhnicheskaya Fizika, Vol. 61, No. 4, pp. 201–210, July–August, 2020. Original article submitted December 11, 2019; revision submitted February 10, 2020; accepted for publication March 2, 2020.
*Corresponding author.

 

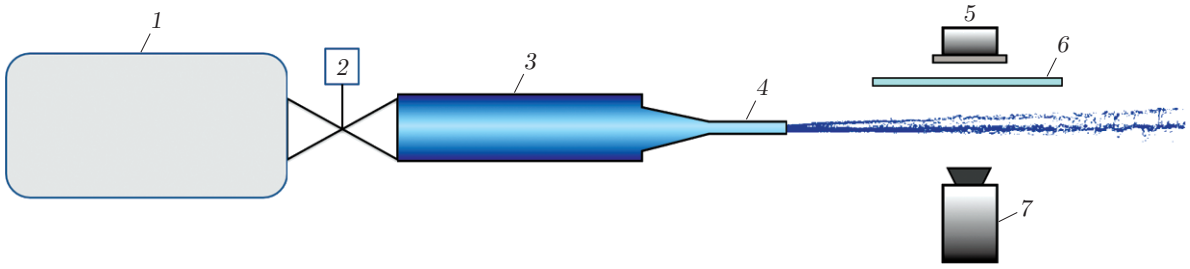


**Fig. 1.** Schematic of the experimental setup: (*1*) pressure tank; (*2*) electromagnetic valve; (*3*) ejection pipe; (*4*) nozzle; (*5*) light source; (*6*) frosted glass; (*7*) high-speed camera.

Middleman [8] and Goldin et al. [9] applied the linear instability theory method and predicted the low-speed laminar viscoelastic jet to be less stable than the Newtonian jet. The nonlinear effect was speculated to arise from the generation of normal stresses in the shear flow prior to ejection of the jet. This is inconsistent with most experiments because the viscoelastic jet generally takes a longer time to break up into droplets than the Newtonian jet [10]. Goren and Gottlieb [11] used the linear instability theory to analyze the surface-tension-driven breakup of viscoelastic liquid jets. They found that the axial elastic tension can produce a significant stabilizing effect if the stress relaxation time constant is sufficiently large. Ruo et al. [12] performed a complete linear stability analysis to study the response of unrelaxed elastic tension to the onset of three-dimensional instability in viscoelastic jets. They predicted that novel oscillating non-axisymmetric modes emerge because of stimulation by elastic energy relaxation causing a variety of asymmetrical deformations. Yarin [13] applied a quasi-one-dimensional method to investigate axial stress stabilization effects on the liquid jet and found that the axial stress in the jet would be larger than the dynamic pressure of air if the elastic modulus is large enough. At the nonlinear stage, the growth of bending disturbances of a polymeric liquid jet is drastically slowed down under the action of internal stresses related to elongation of the jet axis. A small number of high-molecular-weight additives in low-viscosity liquids suppress (or retard) liquid atomization, e.g., as observed in experimental results of Hoyt et al. [14]. Jet breakup is accompanied by the formation of filaments linking all the droplets together. The polymers in the solution reduce, dampen, or eliminate small-scale surface disturbances in the jet, while not reducing but even amplifying larger-scale motions. Keshavarz et al. [15] experimentally investigated the air-assisted atomization mechanisms of viscoelastic fluids, namely, the Kelvin–Helmholtz, Rayleigh–Taylor, and Rayleigh–Plateau instabilities responsible for the three breakup regions. They also found that viscoelasticity monotonically increases the average droplet size, with the distribution of droplet sizes about the mean value uniquely determined by a broad gamma distribution with $n = 4$.

In summary, the previous research has been mainly focused on the capillary breakup of viscoelastic jets. Little experimental work has been done on the development of interfacial disturbances, as well as of the primary breakup morphologies of a viscoelastic jet. Due to the mathematical complexity in dealing with nonlinear rheological constitutive equations, the theoretical and numerical works are relatively limited. A detailed analysis of a high-speed viscoelastic fluid jet is also limited by appropriate methods.

To shed more light on this issue, the high-speed photography was used to study the detailed characteristics of the viscoelastic jet breakup.

## 1. METHODOLOGY

The experiments were conducted at room temperature (approximately 20°C) and normal atmospheric pressure. The liquid jet experimental rig shown in Fig. 1 includes a liquid-filled 50-ml ejection pipe, a cylindrical nozzle, a 2-liter pressure tank filled with compressed air, and an electromagnetic valve. The piston of the ejection pipe is driven by the pressure differential from the pressure tank. The ejection pipe and pressure tank are connected by the electromagnetic valve whose response time is 10 ms. The ejection pipe is projected horizontally across the field of view of the high-speed camera. The field of view is illuminated by an 800-W LED lamp. A frosted glass is used to ensure uniform brightness. The camera (Phantom v2511) with a sampling rate of 48 000 fps was used to capture the spatio-temporal behavior of the liquid jet. The diameter of the cylindrical nozzle was 1.0 mm, and the aspect

Rheological properties of test liquids

| Liquid | $c$, % | $\eta \cdot 10^{-2}$, ml/g | $c/c^*$ | $\eta_s$, mPa·s | $\eta_0$, mPa·s | $\sigma$, mN/m | $\lambda_{\text{eff}}$, ms |
|---|---|---|---|---|---|---|---|
| PEO solution: | | | | | | | |
| $10^6 M_v$ | 0.05 | 5.72 | 0.31 | 1 | 1.21 | 62.3 | 0.88 |
| $2 \cdot 10^6 M_v$ | 0.05 | 5.72 | 0.48 | 1 | 1.41 | 60.9 | 4.12 |
| $5 \cdot 10^6 M_v$ | 0.01 | 5.72 | 0.18 | 1 | 1.45 | 60.7 | 5.11 |
| $5 \cdot 10^6 M_v$ | 0.02 | 5.72 | 0.35 | 1 | 1.61 | 61.2 | 7.85 |
| $5 \cdot 10^6 M_v$ | 0.05 | 5.72 | 0.88 | 1 | 4.96 | 60.8 | 14.31 |
| Glycerol solution | 60.00 | — | — | — | 10.02 | 51.6 | — |
| Purified water | — | — | — | — | 1.00 | 72.1 | — |

ratio of the nozzle was 5. Four observation windows were set up to explore the liquid jet breakup morphologies at different distances, i.e., at 0–180 mm (window I), 180–360 mm (window II), 360–540 mm (window III), and 100–130 mm (window IV) from the nozzle tip along the liquid jet axis.

The concentrations of the polyethylene oxide (PEO) solutions with different molecular weights $M_v$ and their rheological properties are compared to the tested Newtonian fluids in the table. The surface tension $\sigma$ was measured by using a Dataphysics OCA20 surface-tension tester with an uncertainty of 1%, and the shear viscosity $\eta_0$ was measured by an Antonpa MCR302 rheometer with an uncertainty of 0.1%. The effective relaxation time $\lambda_{\text{eff}}$ was evaluated by the following formula [16]:

$$\lambda_{\text{eff}} = 0.463 \frac{\eta M_w \eta_s}{N_{\text{A}} k_{\text{B}} T} \frac{c}{c^*}, \qquad 0.01 \leqslant \frac{c}{c^*} \leqslant 1.00. \tag{1}$$

Here $\eta$ is the intrinsic viscosity of the polymer, $\eta_s$ is the solvent viscosity, $N_{\text{A}}$ is the Avogadro number, $k_{\text{B}}$ is the Boltzmann constant, $T$ is the temperature of the solution, $c$ is the polymer concentration, $c^*$ is the critical overlap concentration, and $M_w$ the mass-average molecular weight (roughly equivalent to the viscosity-average molecular weight $M_v$). For a fluid with a low viscosity, the analysis of the Rayleigh breakup of an inviscid fluid jet is appropriate. The characteristic time scale for breakup is [15]

$$t_R = \sqrt{\rho R_0^3 / \sigma}\,,$$

where $\rho$ is the liquid density, $R_0$ the cross-sectional radius of the jet, and $\sigma$ is the surface-tension coefficient. The dimensionless Deborah number (De) and Reynolds number (Re) are defined by the formulas

$$\text{De} = \frac{\lambda_{\text{eff}}}{t_R} = \frac{\lambda_{\text{eff}}}{\sqrt{\rho R^3/\sigma}}\,, \qquad \text{Re} = \frac{\rho v R}{\mu}.$$

## 2. RESULTS AND DISCUSSIONS

The breakup characteristic of polymeric solution jets with the Reynolds number range Re = 6100–70 700 and Deborah number range De = 0.2–3.5 are studied. The morphological differences between purified water, glycerol solution, and PEO solution (with the molecular weight $M = 5 \cdot 10^6 M_v$ and concentration $\bar{c} = 2 \cdot 10^{-4}$) jets escaping from the nozzle with a velocity of 76 m/s are considered, as well as the structure of PEO solution jets ($M = 5 \cdot 10^6 M_v$ and $\bar{c} = 2 \cdot 10^{-4}$) with jet velocities of 47, 68, and 87 m/s. The diameters of the central liquid column and principal liquid filaments are studied as functions of the jet velocity.

### *2.1. Morphological Differences between the Newtonian and Viscoelastic Liquid Jets*

The liquid jets of Newtonian fluids (purified water and glycerol solution) and polymer (PEO) solution ($M = 5 \cdot 10^6 M_v$ and $\bar{c} = 2 \cdot 10^{-4}$) jets observed through windows I, II, and III for the jet velocity of 76 m/s are shown in Fig. 2. The purified water and glycerol solution jets are developed from an initial transparent undisturbed laminar region to a blurry disturbed region where the flow status inside the jet is turbulent. The disturbance waves grow spatially and temporally with notable growth rates. A divergence angle could be discriminated along the jet

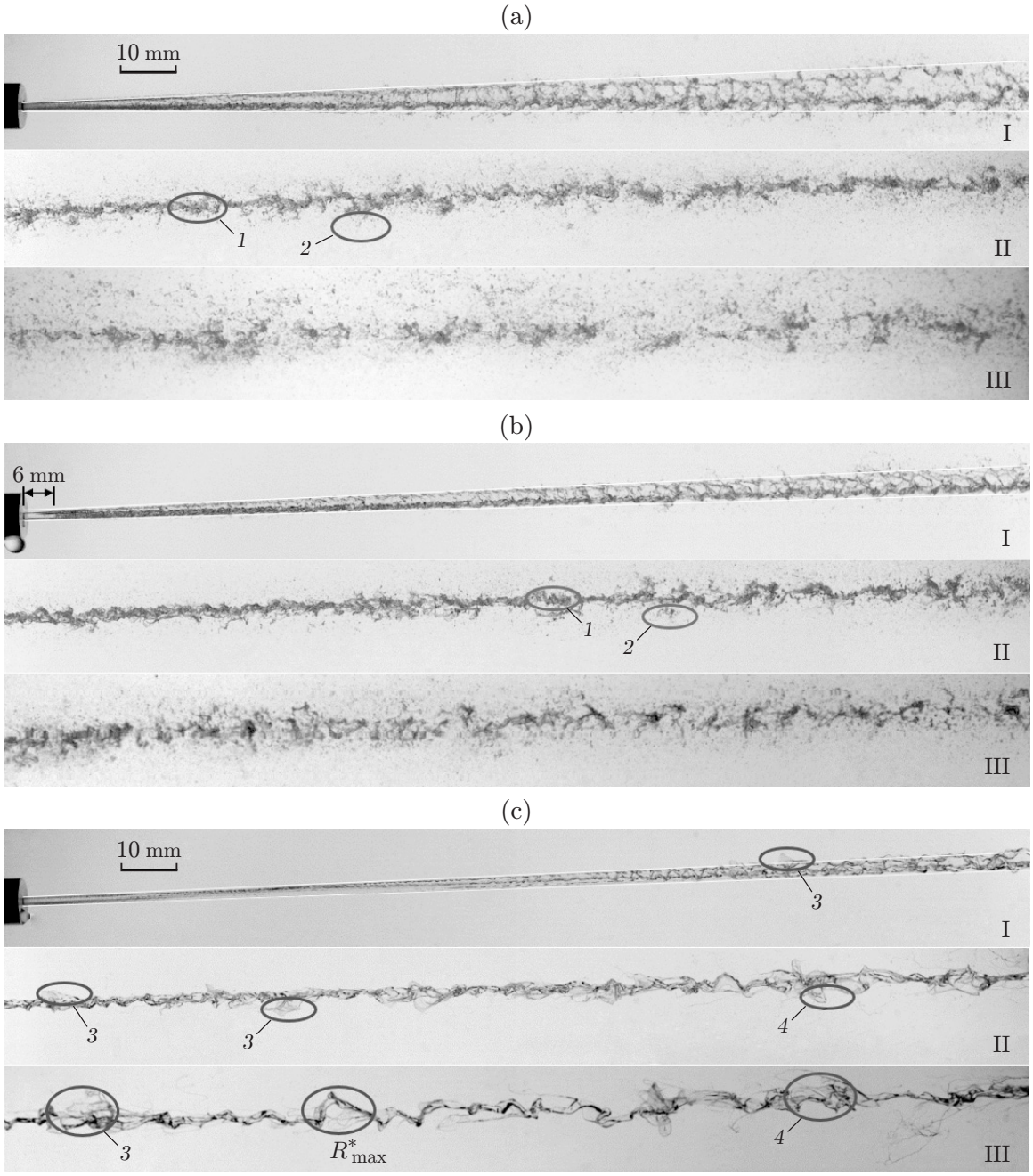


**Fig. 2.** Liquid jets escaping with a velocity of 76 m/s from the nozzle 1 mm in diameter: (a) purified water; (b) glycerol solution; (c) PEO solution ($M = 5 \cdot 10^6 M_v$ and $\bar{c} = 2 \cdot 10^{-4}$); windows I–III are denoted respectively; (*1*) main droplets; (*2*) satellite droplets; (*3*) liquid films; (*4*) liquid filaments.

direction. The jet breakup at a certain location leads to the formation of large main droplets. Subsequently, these droplets break up into smaller (satellite) droplets under the action of aerodynamic forces. This process is called secondary atomization.

In the purified water case, the disturbed region is developed immediately at the nozzle exit. The divergence angle of the jet is approximately 2.5° (window I in Fig. 2a). The liquid column of the purified water jet is seen to be absolutely disrupted in window II, where the main droplets and satellite droplets are observed. A great deal of tiny droplets emerge in window III, indicating full atomization of the liquid.

In the glycerol solution case, the disturbed region is developed at a distance of 6 mm from the nozzle exit. The divergence angle of the jet is approximately 1.5° (window I in Fig. 2b). The liquid column is not disrupted completely in window II. A larger number of the main droplets and fewer satellite droplets are observed as compared to the purified water case. In summary, the degree of liquid fragmentation is lower than that in the purified water case with the same jet velocity. The result is consistent with the conclusion from previous publications: viscosity suppresses the growth of the disturbances.

The polymer solution jet is exceptionally stable as compared to the Newtonian fluid jets. The divergence angle is only 0.5°, which is much smaller than that of the glycerol solution. The undisturbed laminar region is maintained at least 50 mm away from the nozzle exit. The liquid jet maintains a rather smooth cylindrical shape, indicating that the growth of the disturbances is substantially suppressed by polymers. Liquid films connected to the central liquid column are observed, and no satellite droplets emerge from the jet surface in window I. The liquid column of the jet is still successive within the observation window II, and no satellite droplets appear along the jet surface. Instead, both liquid films and thin filaments are peeled away from the jet surface, and they are still connected to the liquid column. A twisted liquid column with large amplitude emerges. In window III, the liquid column is still successive even though the ratio of the disturbance amplitude to the initial jet diameter exceeds 4. This fact evidences the unrelaxed elastic tension along the jet direction, and we infer that this large-amplitude disturbance is a novel oscillating mode predicted by Ruo et al. [12]. Large films and slender filaments linked to the liquid column surface are observed.

### *2.2. Breakup Characteristics of Polymer Solution Jets with Different Jet Velocities*

Figure 3 shows the PEO solution jets ($M = 5 \cdot 10^6 M_v$ and $\bar{c} = 2 \cdot 10^{-4}$) escaping with velocities of 47, 68, and 87 m/s. For the jet velocity of 47 m/s, the liquid column remains cylindrical (window I in Fig. 3a). Small-scale disturbances appear along the jet surface; however, these disturbances are suppressed because the jet surface becomes smooth again further downstream. The disturbance amplitude increases at the later part of the jet (window II), and an uneven liquid column appears at the downstream of the jet. After that, the disturbances evolve spatially, and a twisted liquid column with large disturbance amplitude is observed (window III).

The morphology of the polymer solution jet with the jet velocity of 68 m/s is shown in Fig. 3b. It seems that the small-scale disturbances are much closer to the nozzle tip than those in the 47 m/s case. The disturbances grow spatially, and small pieces of liquid films are peeled off from the liquid column (window I). The disturbance amplitude increases remarkably. The disturbance wave length becomes greater, and larger pieces of films appear (window II). Again, a twisted liquid column with more liquid films is observed in window III.

The morphology of the polymer solution jet with the jet velocity of 87 m/s is shown in Fig. 3c. It is observed that the disturbances grow fiercely, giving rise to a hollow jet formation with a divergence angle (window I). The jets are still successive, though a few films appear along the jet surface. Both large pieces of liquid films and a lot of slender liquid filaments appear in window II. A twisted liquid column with even larger disturbance amplitude is seen in window III. The filaments are stretched even longer and slenderer. They cross with each other and form a net-like structure.

The mechanism of enhanced stability of viscoelastic fluid jets is regarded to be a result of unrelaxed stresses generated at the nozzle before the liquids were ejected, because large deformation of polymeric molecules occurs under the high shear rate or extensional rate during their squeezing inside the nozzle. Such residual stresses can persist along the jet for a large distance, which depends on the relaxation time and jet velocity. Although the stresses decay exponentially with increasing distance from the nozzle, they produce a substantial stabilizing effect on the initial growth of disturbances. The twisted liquid column with large disturbance amplitudes is the proof

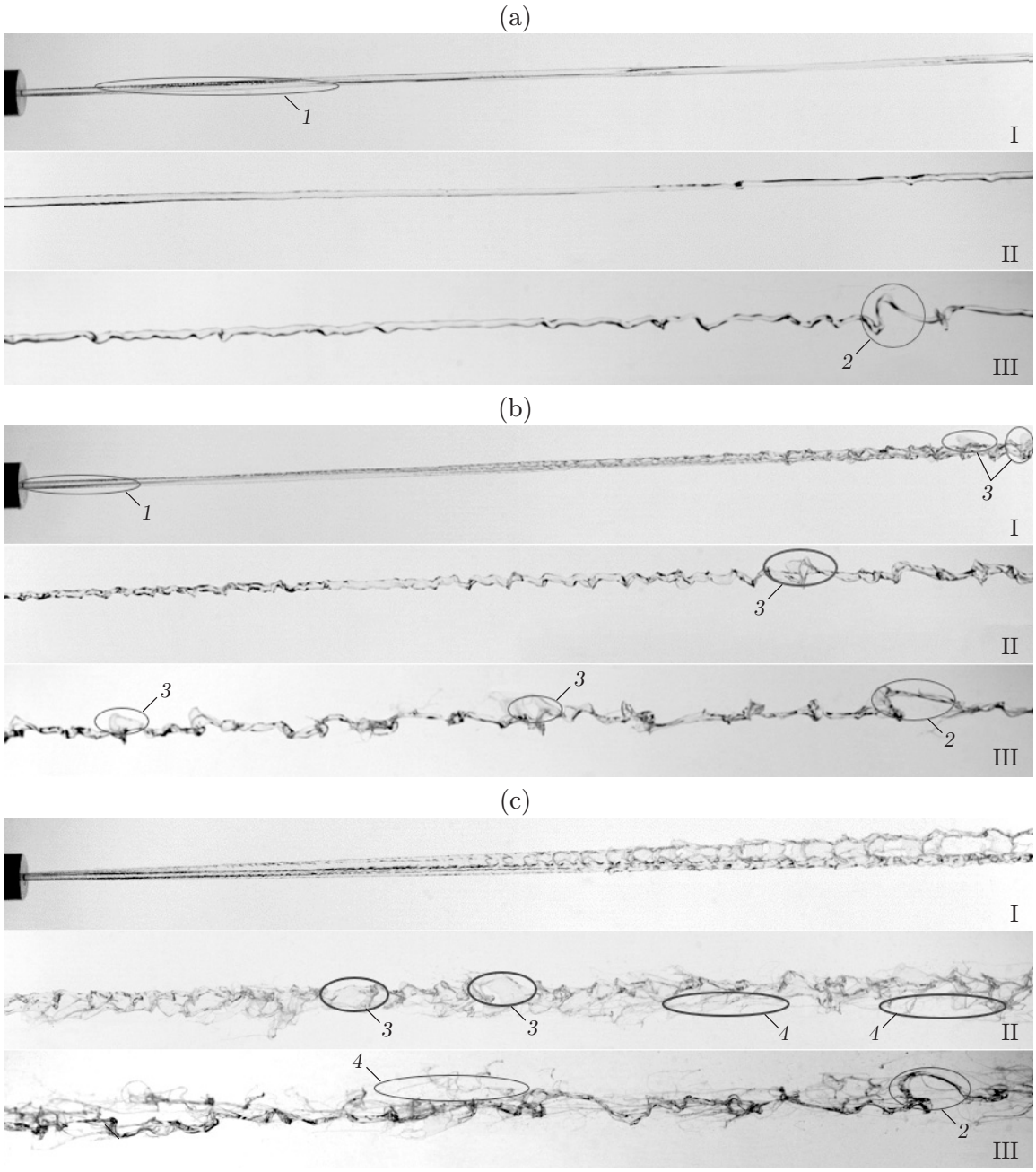


**Fig. 3.** PEO solution jets ($M = 5 \cdot 10^6 M_v$ and $\bar{c} = 2 \cdot 10^{-4}$) escaping with velocities of 47(a), 68 (b), and 87 m/s (c): windows I–III are indicated respectively; (*1*) small-scale disturbances; (*2*) twisted liquid column; (*3*) liquid films; (*4*) liquid filaments.

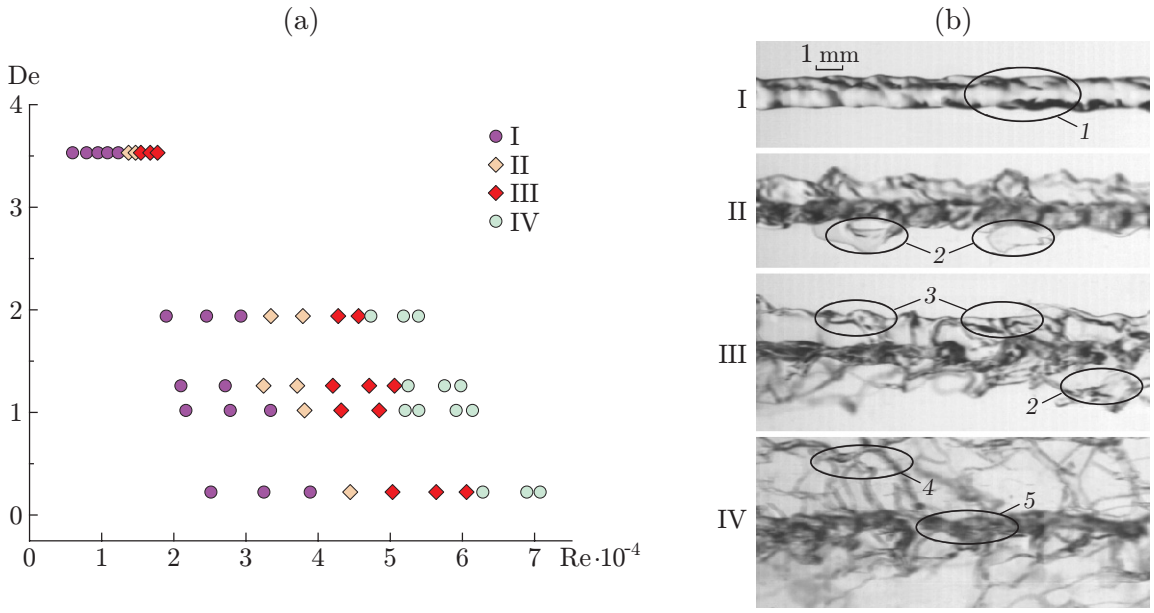


**Fig. 4.** Breakup pattern diagram for the polymer solution jet (a) and broken jets (b): (I) no liquid films or filaments; (II) liquid films; (III) liquid films and filaments; (IV) net-like filament pattern; (*1*) multimodal disturbances; (*2*) liquid films; (*3*) liquid filaments; (*4*) principal liquid filament; (*5*) central liquid column.

of unrelaxed axial tension. Therefore, shear forces emerge due to the relative motion between the jet and the surrounding gas. Films and filaments are formed under the action of shear forces. Extensional stresses are formed in the nonlinear necking process, resulting in large deformations of polymeric molecules. The extensional stresses inhibit the capillary-driven pinch action. Consequently, they retard the subsequent breakup process, while larger liquid films and longer filaments are formed along the jet.

### *2.3. Breakup Patterns of Viscoelastic Jets*

The polymer solution jets exhibit distinctive morphologies at different jet velocities. To classify their breakup patterns, the observation window IV was placed 10 cm away from the nozzle tip. The jet morphologies of the PEO solutions with different concentrations and $M_v$ values reveal four kinds of breakup patterns: (1) pattern with no liquid films or filaments; (2) liquid film pattern; (3) pattern with films and filaments coexistence; (4) net-like filament pattern. The breakup of the PEO solution jet ($M = 5 \cdot 10^6 M_v$ and $\bar{c} = 10^{-4}$) with different velocities of jet exhaustion from the nozzle was studied.

A qualitative phase diagram is obtained based on the four breakup patterns (Fig. 4). It is observed that the breakup of the polymer solution jet is more difficult with increasing De and decreasing Re owing to longer times of elastic stress relaxation.

The characteristics of the pattern with no liquid films or filaments can be formulated as follows: the liquid column is successive with axisymmetric or antisymmetric disturbances on the jet surface. The liquid column is almost homogeneous, and the disturbance amplitude is small. No liquid films and filaments are peeled off from the jet surface. In the presence of liquid films, the liquid column diameter remains equal to the initial jet size, and a few massive liquid films are peeled off occasionally from the jet surface under the action of the drag force induced by the difference in the gas and liquid velocities. Almost no liquid filaments are formed. In the presence of both liquid films and filaments, thick liquid films and massive filaments are frequently peeled off from the jet surface. The disturbance amplitude becomes rather large, and the liquid column diameter becomes much thinner than the initial jet diameter. At the net-like pattern stage, long and slender liquid filaments are observed along the jet surface; the filaments cross each other, forming a three-dimensional net-like structure.

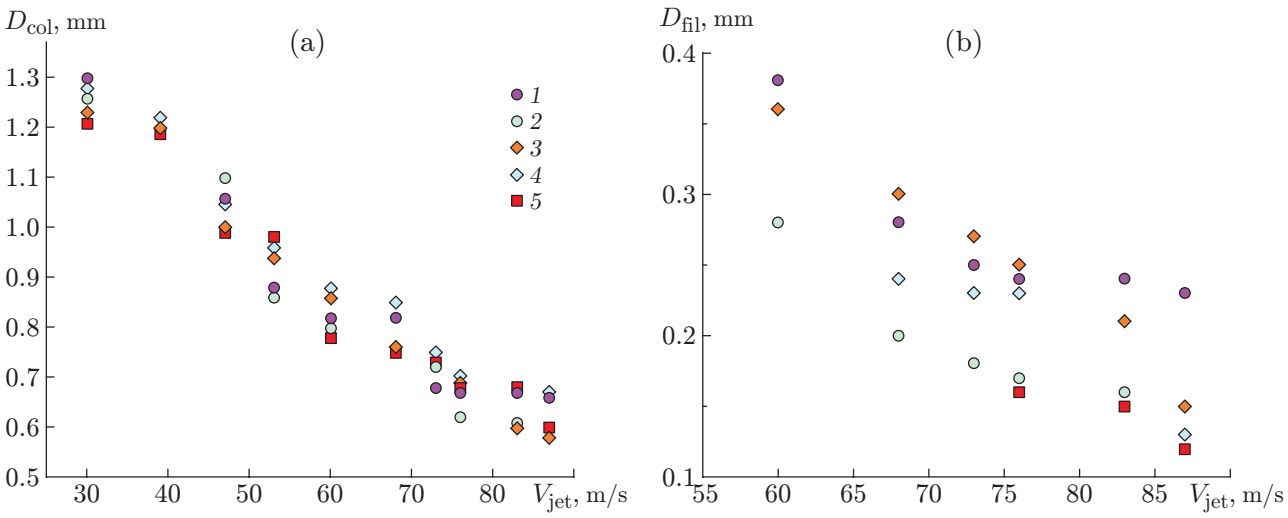


**Fig. 5.** Diameters of the central liquid column $D_{col}$ (a) and principal liquid filament $D_{fil}$ (b) in the PEO solution versus the jet velocity $V_{jet}$: (*1*) $M = 10^6 M_v$ and $\bar{c} = 5 \cdot 10^{-4}$; (*2*) $M = 2 \cdot 10^6 M_v$ and $\bar{c} = 5 \cdot 10^{-4}$; (*3*) $M = 5 \cdot 10^6 M_v$ and $\bar{c} = 10^{-4}$; (*4*) $M = 5 \cdot 10^6 M_v$ and $\bar{c} = 2 \cdot 10^{-4}$; (*5*) $M = 5 \cdot 10^6 M_v$ and $\bar{c} = 5 \cdot 10^{-4}$.

### *2.4. Variation Trends of the Diameter of the Central Liquid Columns and Principal Liquid Filaments*

The diameter of the central liquid column is defined as $D_{col}$, and the diameter of the principal liquid filament is defined as $D_{fil}$. The values of $D_{col}$ and $D_{fil}$ for PEO solution jets escaping from the nozzle with different velocities are measured. The diameters are found by counting the number of pixels occupied by the central liquid column or principle liquid filament in images taken by a high-speed camera. There are 50 sampling points in one captured photo along the jet direction; the average values of the measuring points are calculated and treated as the final result for the diameter. The absolute error of the measuring sampling comes from distinguishing the border of the central liquid column or principle liquid filament (the absolute error for each border is 2 pixels). Therefore, the absolute error of determining both borders is 4 pixels, (37 $\mu$m with allowance for magnification of the high-speed camera).

The variation trends of the diameter of the central liquid columns and their principal filaments $D_{col}$ and $D_{fil}$ are shown in Fig. 5. The diameters $D_{col}$ and $D_{fil}$ are seen to decrease with an increase in the liquid jet velocity. Moreover, for the same jet velocity, the diameter of the filaments decreases with increasing both molecular weight and concentration of polymer solutions. We inferred that the extensional stress formed in the capillary-driven pinch process is larger in PEO solutions with higher molecular weights and concentrations; therefore, the filaments are stretched and become thinner.

## CONCLUSIONS

The breakup morphologies of dilute polymer solution jets were studied experimentally. The main findings can be summarized as follows.

With small concentrations of the polymer added to the solution, the liquid jet shows notably higher stability than the Newtonian fluid jets. The liquid jet column remains almost cylindrical even at large distances from the nozzle. Small-scale disturbances are suppressed evidently by the polymer, and a twisted liquid column oscillating with large amplitude emerges. The breakup morphology of the polymer solution jet is quite different from that of the Newtonian fluid jets. As the Reynolds number increases and reaches a critical value, liquid films and filaments are peeled off successively from the liquid jet column. At high jet velocities, crossing filaments form a net-like structure.

The unrelaxed axial tension produces a substantial stabilizing effect on the initial growth of disturbances. Films and filaments emerge under the action of shear forces. Extensional stresses are formed in the nonlinear necking process because large deformations of polymeric molecules arise there. As a result, the breakup process is retarded; larger liquid films and longer filaments are formed.

Four different breakup patterns are distinguished. The diameters of the central liquid columns and principal liquid filaments decrease with increasing jet velocity. For the same jet velocity, the diameter of the principal filaments decreases with an increase in the molecular weight and concentration of the polymer solution.

Financial Support for this work was provided by the National Key R&D Program of China (Grant No. 2018YFB0606103).

## REFERENCES

1. O. Arnolds, H. Buggisch, D. Sachsenheimer, and N. Willenbacher, "Capillary Breakup Extensional Rheometry (CaBER) on Semi-Dilute and Concentrated Polyethyleneoxide (PEO) Solutions," Rheol. Acta **49** (11), 1207–1217 (2010).
2. N. F. Morrison and O. G. Harlen, "Viscoelasticity in Inkjet Printing," Rheol. Acta **49** (6), 619–632 (2010).
3. V. M. Kulik, S. V. Rodyakin, I. Lee, and H. H. Chun, "Deformation of a Viscoelastic Coating under the Action," Exp. Fluids **38** (5), 648–655 (2005).
4. R. P. Mun, B. W. Young, and D. V. Boger, "Atomisation of Dilute Polymer Solutions in Agricultural Spray Nozzles," J. Non-Newtonian Fluid Mech. **83** (1), 163–178 (1999).
5. T. Han, A. L. Yarin, and D. H. Reneker, "Viscoelastic Electrospun Jets: Initial Stresses and Elongational Rheometry," Polymer. **49** (6), 1651–1658 (2008).
6. J. Eggers and E. Villermaux, "Physics of Liquid Jets," Rep. Progress Phys. **71** (3), 036601 (2008).
7. M. Negri and H. K. Ciezki, "Atomization of non-Newtonian Fluids with an Impinging Jet Injector: Influence of Viscoelasticity on Hindering Droplets Formation," in *Proc. of the 46th AIAA/ASME/SAE/ASEE Joint Propulsion Conf., Nashville, July 25–28, 2010* (AIAA, 2010), pp. 1–11.
8. S. Middleman, "Stability of a Viscoelastic Jet," Chem. Eng. Sci. **20** (12), 1037–1040 (1965).
9. M. Goldin, J. Yerushalmi, R. Pfeffer, and R. Shinar, "Breakup of a Laminar Capillary Jet of a Viscoelastic Fluid," J. Fluid Mech. **38** (4), 689–711 (1969.).
10. M. Gordon, J. Yerushalmi, and R. Shinnar, "Instability of Jets of non-Newtonian Fluids," J. Rheol. **17**, 303–324 (1973).
11. S. L. Goren and M. Gottlieb, "Surface-Tension-Driven Breakup of Viscoelastic Liquid Threads," J. Fluid Mech. **120**, 245–266 (1982).
12. A. C. Ruo, F. Chen, C. A. Chung, and M. H. Chang, "Three-Dimensional Response of Unrelaxed Tension to Instability of Viscoelastic Jets," J. Fluid Mech. **682**, 558–576 (2011).
13. A. L. Yarin, *Free Liquid Jets and Films: Hydrodynamics and Rheology* (Longman Sci. and Tech., Haifa, 1993).
14. J. W. Hoyt, J. J. Taylor, and C. D. Runge, "The Structure of Jets of Water and Polymer Solution in Air," J. Fluid Mech. **63** (4), 635–640 (1974).
15. B. Keshavarz, V. Sharma, and E. C. Houze, "Studying the Effects of Elongational Properties on Atomization of Weakly Viscoelastic Solutions using Rayleigh Ohnesorge Jetting Extensional Rheometry (ROJER)," J. Non-Newtonian Fluid Mech. **222** (8), 171–189 (2015).
16. B. Keshavarz, E. C. Houze, J. R. Moore, et al., "Ligament Mediated Fragmentation of Viscoelastic Liquids," Phys. Rev. Lett. **117** (15), 154502 (2016).